Nano Research
2019, 12(6): 1327–1331

ISSN 1998-0124 CN 11-5974/O4
https://doi.org/10.1007/s12274-019-2284-0

Research Article

Fabrication of NiFe layered double hydroxide with well-defined laminar superstructure as highly efficient oxygen evolution electrocatalysts

Hao Zhang, Haoyi Li, Bilal Akram, and Xun Wang (✉)

Department of Chemistry, Tsinghua University, Beijing 100084, China

Received: 5 December 2018 / **Revised:** 31 December 2018 / **Accepted:** 1 January 2019

ABSTRACT

Structure–activity relationship (SAR) is the key problem of nanoscience, thus to fabricate novel and well-defined nanostructure will provide a new insight on catalyst preparation method. Highly active and low cost electrocatalysts for oxygen evolution reaction (OER) are of great importance for future renewable energy conversion and storage. Herein, NiFe-based layered double hydroxides with laminar structure (NFLS) were successfully fabricated via a one-step hydrothermal approach by using sodium dodecyl sulfate as surfactant. The as-fabricated NFLS showed a well-defined periodic layered-stacking geometry with a scale down to 1-nm. Benefitting from the unique structure, NFLS exhibited an excellent catalytic activity towards OER with current densities of 10 $mA{\cdot}cm^{-2}$ at overpotential of 197 mV. The synergistic effect of Ni and Fe plays a key role in electrode reactions. The present work provides a new insight to improve the OER performance by rational design of electrocatalysts with unique structures.

KEYWORDS

layered double hydroxide, structure–activity relationship, ultrathin nanostructure, electrocatalysis, oxygen evolution reaction

One of the research directions of nanoscience is to understand the interaction between structure and function, which has enabled scientists to extend the synthesis strategies and potential applications of nanostructures [1]. The physical and chemical properties vary greatly when the dimensions of nanostructures are down to 1-nm scale [2], thus the controllable and convenient fabrication of ultrathin nanocrystals is highly desirable for potential applications in different fields. Among various kinds of nanostructures, laminar superstructures, which present periodic multi-level layered-stacking geometry, attract a great attention owing to high specific surface area and excellent stability [3]. Layered double hydroxide (LDH), composed of positively charged metal layers and inserted anions and solvation molecules [4], is one of the best building block of laminar superstructures. Ordinary LDH bulks suffer from the lack of exposed active sites and are hardly to get a better catalytic performance, thus it is an urgent need to design and synthesize ultrathin LDH nanostructures with well-defined construction and morphology. The top-down exfoliation approach is commonly used to obtain LDH nanosheets [5–8]. However, the refined morphology of as-synthesized LDH nanosheets obtained by exfoliation cannot be controlled precisely, as the high charge density of LDHs makes it harder to be exfoliated into monolayer [4]. Moreover, LDH exfoliation process has sophistications associated with it, such as several days of inert atmospheric protection [9], which may limit the industrial applications in the area of electrochemistry.

Contrarily the exfoliation-free bottom-up methods provide another convenient approach to get LDH nanostructures [10]. In the bottom-up synthesis route, surfactants such as sodium dodecyl sulfonate (SDS) are introduced to form micelles as nanoreactors in which LDH nanostructures are grown through confined space and nutrients [4]. Therefore in the rational design of LDH ultrathin nanostructure, the chief aim of the researchers is to control the structure and morphology by employing proper surfactants.

Owing to their unique structural features LDHs are regarded as best alternates to noble metal electrocatalysts. In the proceeding lines we will briefly overview the electrochemical catalytic performance of LDH superstructure especially the electrochemical oxygen evolution reaction (OER). As we all know that electrochemical water splitting has been considered to be a promising technology for the advanced renewable energy conversion to replace fossil fuels [11, 12]. In this context OER is considered to be the key process of water splitting with uphill potential and slow kinetics, in which the catalysts need to overcome a substantial overpotential to reach the desired current densities [13]. Thus to design and fabricate highly efficient OER catalysts gradually rises to the core issue of electrochemistry. Noble metal oxides such as IrO_2 and RuO_2 are considered to be the best OER electrocatalysts for water splitting in both alkaline and acidic media. However the high cost and low abundance strictly limit their extensive use [14]. Thus the first-row transition metal compounds such as oxides [15–19], hydroxides [5, 20, 21], nitrides [22–24], selenides [25, 26], phosphates [27, 28] and phosphides [29, 30] have been largely used as alternate OER electrocatalysts because of their low cost, high abundance and remarkable efficiency. Among these catalysts, layered double hydroxides (LDHs) have been widely investigated for their unique 2-dimensional lamellar structure and reliable catalytic performance in OER [6, 8, 31–36].

Taking the above contents into account, nickel-iron LDH nanostructure are regarded as the most promising OER catalysts due to their special electronic configuration which arises as a result of Fe incorporation into α-$Ni(OH)_2$/γ-NiOOH lattices [21, 37]. Moreover Ni–O and Fe–O bond distances are comparable, thus these two metals can easily replace each other and form edge-sharing [FeO_6] and [NiO_6] octahedral [38]. Compared with pure nickel oxyhydroxides, Fe incorporation leads to a dramatic increase in OER performance

Address correspondence to wangxun@mail.tsinghua.edu.cn

by inducing partial-charge transfer [39, 40]. Herein, we demonstrate a bottom-up self-assembly process of Ni-Fe-LDH-based laminar superstructure (NFLS) formation via a one-step hydrothermal method. The composition, morphology and OER performance were being investigated in detail. The as-synthesized NFLS presents a long-range ordered superlattice pattern (Scheme 1). SDS plays a key role in regulating the formation process of laminar superstructure. As for the OER performance, NFLS showed an overpotential of 197 mV to reach a current density of 10 mA·cm^{-2} on glassy carbon electrodes (GCE) without any iR correction, which is superior to many reported catalysts (Table S1 in the Electronic Supplementary Material (ESM)). Especially, the influence of NFLS structure on OER activity was being analyzed to reveal the structure–activity relationship, which may provide an insight for future electrocatalysts fabrication.

In a typical synthesis, NFLS was obtained in aqueous solution via a single-step hydrothermal process by using nitrates precursors. The developed method is general in case of precursors as chlorides and sulphates can also get results in the similar products. When the reaction temperature increased from room temperature to 120 °C the product was nanoparticles and amorphous nanosheets, along with a small quantity of laminar regions (Fig. S1(a) in the ESM). During the hydrothermal process, laminar regions were enlarged and disordered amorphous nanosheets regions disappeared (Figs. S1(b)–S1(d) in the ESM). Finally all the intermediate nanostructures were converted into the well-organized laminar superstructures with columnar outlines (Figs. 1(a) and 1(b), and Fig. S2 in the ESM). The as-synthesized columnar NFLS had diameter of 50–100 nm and length of several hundreds of nanometers. The columnar outlines were further transformed to larger nanosheets when the reaction time was prolonged to 8 h, and the basic building blocks remain the same (Figs. 1(c) and 1(d)). As-synthesized NFLS was composed of ultrathin nanoribbons with a long-range ordered arrangement. The laminar structure has a single-layer thickness of 2.0 nm and a uniform interlayer spacing of 1.8–3.0 nm, which was negatively correlated with reaction time. Considering that the length of dodecyl sulfonic anions (DS^- for short) was ~ 1.6 nm, it enlightened us to think that DS^- play a key role in the formation of laminar structure for its particular configuration and size. The scanning transmission electron microscopy (STEM) image and energy-dispersive X-ray (EDX) spectra (Figs. 1(e) and 1(f)) exhibited the elemental composition and uniform distribution of those elements in NFLS.

A series of controlled experiments were conducted in which sodium dodecyl benzene sulfonate (SDBS) was used instead of SDS. The corresponding products were ultrathin Fe-Ni nanoribbons (NFNR) (Fig. S3 in the ESM), which were exactly similar to the basic building block of NFLS. Based on these observations it can be assumed that sulfonate groups coordinate with the metal cations and dodecyl tails regulate the formation of laminar structure and NFLS were formed by ordered stacking of LDH nanoribbons. OH^- and CO_3^{2-} were gradually released into solution while urea was being decomposed thermally during the fabrication process, thus the growth of NFLS could be precisely controlled. Oppositely, transition metal salts with stronger ligands as anions such as acetate or acetylacetonate could not be used as substrates for NFLS growth as their use results in the formation of nanosheets or nanoparticles with irregular orientation (Figs. S4(a) and S4(b) in the ESM). This might be due to the reason that these ligands bind to metal ions intensively and it becomes difficult for DS^-, OH^- and CO_3^{2-} to coordinate with metal ions hence the ligand–ligand interaction of interlayered DS^- is disturbed. Contrarily, employing Na_2CO_3 instead of urea also led to irregular nanosheets or nanoparticles (Fig. S4(c) in the ESM). Use of stronger bases such as $NH_3{\cdot}H_2O$ or NaOH preferably gives nanoparticles (Figs. S4(d) and S4(e) in the ESM) because strong bases quickly bind to metal cations and hydroxides are directly formed without well-defined morphology.

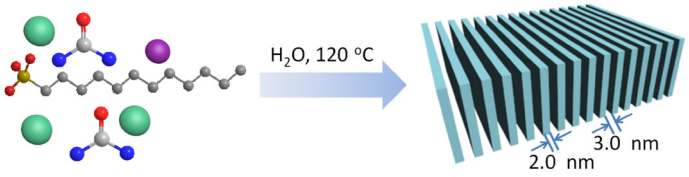

Scheme 1 One pot synthesis strategy of Ni-Fe-LDH-based laminar structure. Color of balls: yellow (sulfur); red (oxygen); blue (nitrogen); gray (carbon); green (nickel ion); purple (ferric ion).

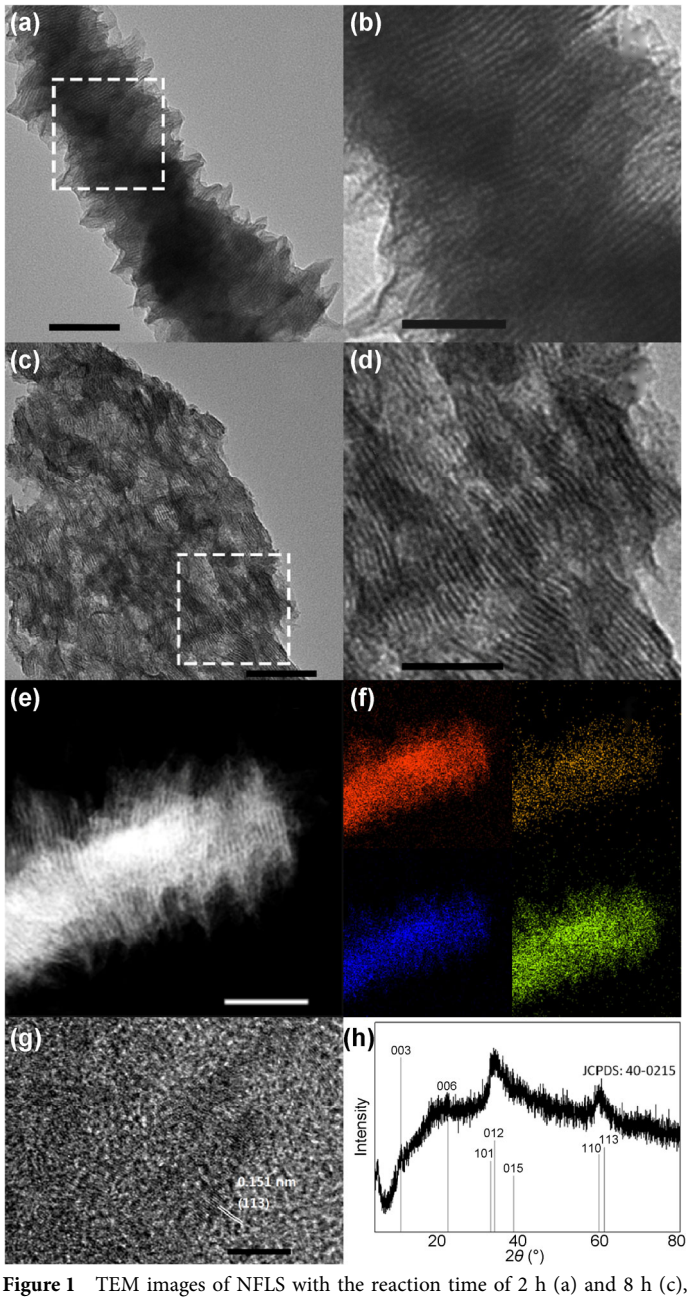

Figure 1 TEM images of NFLS with the reaction time of 2 h (a) and 8 h (c), showing the tubular and platelike profiles separately. (b) and (d) show the enlarged images of white boxes in (a) and (c). (e) STEM and (f) EDX mapping spectra of tubular NFLS, showing the laminar pattern and uniform distribution of O (red), S (yellow), Fe (blue) and Ni (green). (g) HRTEM image of tubular NFLS shows the lattice distance of 0.151 nm, which is indexed to (113) planes of NiFe-LDH. (h) XRD pattern of NFLS and the standard curve of $Ni_{0.75}Fe_{0.25}(CO_3)_{0.125}(OH)_2{\cdot}0.38H_2O$ (JCPDS: 40-0215) (vertical bars). Scale bar: 100 nm (a) and (c); 50 nm (b), (d) and (e); 5 nm (g).

X-ray diffraction (XRD) peaks of NFLS were broaden and hard to fit with any certain crystal structures exactly, though a part of peaks labeled by vertical bars could fit the standard curve of

$Ni_{0.75}Fe_{0.25}(CO_3)_{0.125}(OH)_2{\cdot}0.38H_2O$ (JCPDS: 40-0215), which illustrated that NFLS showed good crystallinity (Fig. 1(h)). Absence of (003) and (006) peaks revealed the nanoribbon building blocks of NFLS with an ultrathin scale at one dimension. Lattice fringes of these crystal planes were also verified by high resolution TEM (HRTEM) visually (Fig. 1(g)). NFLS and NFNR shared similar XRD pattern, which confirmed the same LDH building blocks. The laminar structure contributed to a large specific surface area as revealed by nitrogen adsorption–desorption isotherm (Fig. 2(a)). The Brunauer–Emmett–Teller (BET) surface areas of NFLS was measured to be 78.1 $m^2{\cdot}g^{-1}$, while the reported values for LDH in other relevant literatures were often in the range of 10–60 $m^2{\cdot}g^{-1}$ [41]. The average pore width is 12.3 nm calculated through Barrett–Joyner–Halenda (BJH) desorption curve (Fig. 2(b)). Fourier transform infrared spectra (FT-IR) of NFLS further revealed the existence of DS^- (Fig. 2(c) and Table S2 in the ESM). The bands at 1,248, 1,105 and 977 cm^{-1} were characteristic vibration for OSO^{3-} stretching [42]. Inductively coupled plasma optical emission spectra (ICP-OES) was applied to measure the contents of each element. The ratio of Fe:Ni:S was 2.90:1:0.87, which fixed the XRD pattern of NFLS and further confirmed DS^- coordination.

The X-ray photoelectron spectroscopy (XPS) was used to analyze the valence state of NFLS (Figs. 2(d) and 2(e)). In XPS spectrum, peaks at 723.7 and 711.6 eV stood for Fe^{3+} and 872.9 and 855.1 eV for Ni^{2+} in Ni-Fe layered double hydroxides [7, 43]. The peak at 167.7 eV was indexed to S^{6+}, indicating the existence of dodecyl sulfonate anions in NFLS. Soft X-ray absorption spectra (sXAS) were further conducted to analyze the fine electron of NFLS, NFNR and LDH bulk (Fig. 3). The L3 peaks of Ni were precisely fitted each other. Peaks at 850.7 eV stood for Ni^{2+} and shoulder peaks at 852.7 eV revealed the existence of Ni^{3+}, which was regarded as OER active site. Two peaks appear at Fe L3 edge at 708.4 and 706.6 eV for Fe^{3+} and Fe^{2+} respectively, and Fe^{3+} was the main valence state of iron in NFLS and NFNR. Peaks of Fe^{3+} showed a red-shift of 0.2 eV relative to LDH bulk, qualitatively indicated that the electron density of Fe^{3+} sites has been changed by the cooperation of DS^-, and electrons were transferred from ligands to Fe^{3+} sites compared with LDH bulk [44].

OER performances of NFLS, NFNR, Fe-Ni-LDH bulk as well as commercial IrO_2 were being conducted in a three-electrode system

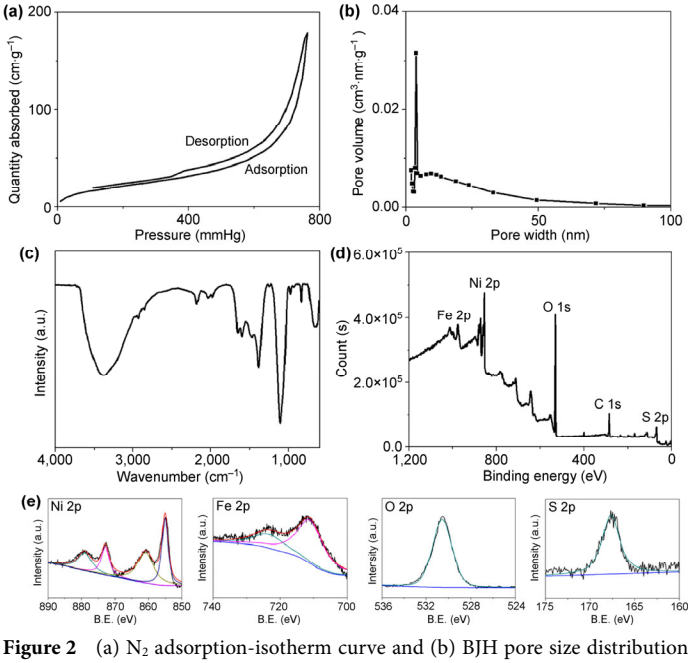

Figure 2 (a) N_2 adsorption-isotherm curve and (b) BJH pore size distribution curve of NFLS. (c) FT-IR spectra of NFLS reveals the existence of DS^- coordination. (d) Overall XPS curve and (e) individual peaks of Ni 2p, Fe 2p, O 2p and S 2p with baseline verification show the valence state of NFLS.

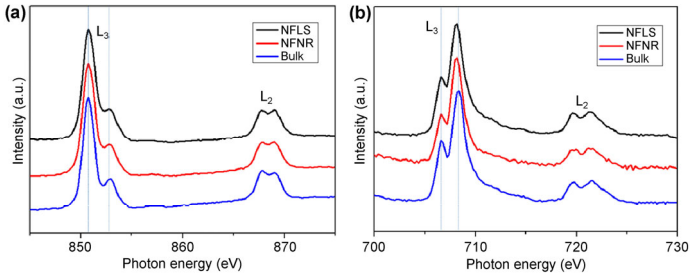

Figure 3 Normalized Ni L-edge (a) and Fe L-edge (b) sXAS patterns of NFLS, NFNR and LDH bulk.

in oxygen-saturated 1 M KOH solution at room temperature. All samples were mixed with carbon powder (Vulcan XC72) with a mass ratio of 4:1 to enhance the conductivity. Figure 3(a) shows the cyclic voltammetry (CV) curve of NFLS. Linear sweep voltammetry (LSV) curves in 1 M KOH with NFLS, NFNR, LDH bulk and IrO_2 as electrocatalysts (Fig. 4(a)) show that the polarization curve of NFLS display a sharp onset potential of OER at ~ 0.42 V (vs. mercuric oxide electrode (MOE)), while LDH bulk and IrO_2 showed higher onset potential at ~ 0.57 and ~ 0.54 V respectively. The shoulder peak located at 0.39 V (vs. MOE) was denoted as the $Ni(OH)_2/NiOOH$ redox characteristics, which indicates Ni^{3+} as the active centers of OER [45, 46]. It could be found that NFLS exhibit an overpotential at 10 $mA{\cdot}cm^{-2}$ of 197 mV, which was much lower than LDH bulk (335 mV), NFNR (277 mV) and IrO_2 (358 mV). Specifically, NFNR present inferior OER performance relative to NFLS, and these differences were caused by the confinement effect of the stacked geometry of NFLS [47, 48]. The Tafel slope of NFLS (Fig. 4(b)) were measured to be 100 $mV{\cdot}dec^{-1}$, smaller than that of NFNR (139 $mV{\cdot}dec^{-1}$) and LDH bulk (129 $mV{\cdot}dec^{-1}$), which indicated that despite sharing similar basic building modules, the laminar structure presents a higher OER rates relative to dissociative nanoribbons.

To further reveal the electrochemistry process on the surface of GCE, electrochemical impedance spectra (EIS) was conducted to unravel the charge transfer resistance of NFLS (Fig. 4(c)). According to EIS curves in Fig. 4, the charge transfer resistance of NFLS exhibited a significant decrease as compared to that of NFNR and LDH bulk. These differences suggest that NFLS exhibit the fastest charge transfer process among all the samples, which might be attributed to the unique layered stacking structures and the interaction between Ni active sites on nearby layers. This was supported by double layer

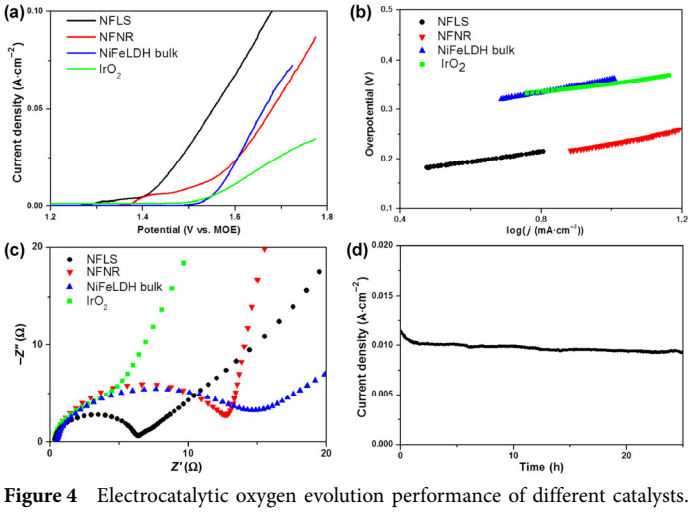

Figure 4 Electrocatalytic oxygen evolution performance of different catalysts. (a) LSV curves of NFLS, NFNR, LDH bulk and IrO_2 for OER at a scan rate of 10 $mV{\cdot}s^{-1}$ in 1 M KOH electrolyte. (b) Tafel slope of all catalysts in 1 M KOH electrolyte. (c) EIS Nyquist plots for different electrocatalysts recorded at an open-circuit voltage. (d) Chronoamperometric response at an overpotential of 300 mV.

capacitance (C_{dl}) of working electrode, which was measured by CV scanning around the open circuit voltage (~ −0.14 V vs. MOE) under different scanning rates (Fig. 5). NFLS showed a capacitance of 0.642 mF·cm^{-2}, while NFNR and LDH bulk showed 0.233 and 0.104 mF·cm^{-2} respectively. The electrochemical surface area (ECSA) is a key evidence to prove the structure–activity relationship of NFLS, for the density of catalytic active sites could be determined by ECSA. ECSA could be calculated via the following equation [49]

$$\mathrm{ECSA} = \frac{C_{\mathrm{dl}}}{20\ \mu\mathrm{F}\cdot\mathrm{cm}^{-2}}\ \mathrm{cm}^2_{\mathrm{ECSA}} \quad (1)$$

NFLS show an ECSA of 32.3 cm^2, which is much larger than NFNR (11.7 cm^2) and LDH bulk (5.2 cm^2).

To better understand the relationship between structure and catalytic activity, OER performance of different samples obtained at different reaction conditions as well as different Fe/Ni ratio was being evaluated. It was obvious that the oxidation peaks at ~ 0.4 V (vs. MOE) were corresponding to $Ni(OH)_2$/NiOOH redox characteristic, and Fe incorporation plays a key role on electronic configuration [21, 37, 38]. It could be seen that FeNi-LDH exhibited higher OER activity than $Ni(OH)_2$ layered structure(Figs. 6(a) and 6(b)). Compared with $Ni(OH)_2$ controlled group, the incorporation of Fe enhanced $Ni(OH)_2$/NiOOH redox peaks on LSV curves, and the OER activity presented a volcano-type shape change, which indicated the synergistic effect between Fe and Ni and a ratio around 1:3 was the preferable composition. Fe^{3+} sites helped the electron transfer of $Ni(OH)_2$/NiOOH transformation and make Ni^{2+} easily to be oxidized, which significantly improved OER performance [38]. However, decrease of Ni sites concentration could influence the current density. Thus there was a most suitable Fe:Ni ratio around 1:3 according to Fig. 5(b). We further founded that OER activity was also affected by the reaction time of hydrothermal process. The function between OER activities and reaction time also showed a volcano-type curve (Figs. 6(c) and 6(d)), indicating that an impeccable layered stacking morphology had a confinement effect and enhanced OER activity.

In summary, the well-defined LDH laminar superstructure as efficient electrocatalysts for OER was fabricated by a single-step bottom-up hydrothermal process. The result demonstrated that the layered stacking structure of NFLS was the key to enhance the OER activity, which was superior to LDH bulks. The optimized NFLS presented a very small overpotential of 197 mV to reach a current density of 10 mA·cm^{-2}. Such a fabrication strategy may provide a valuable insight into rational design of multi-stage superstructures with potential applications in renewable energy conversion field.

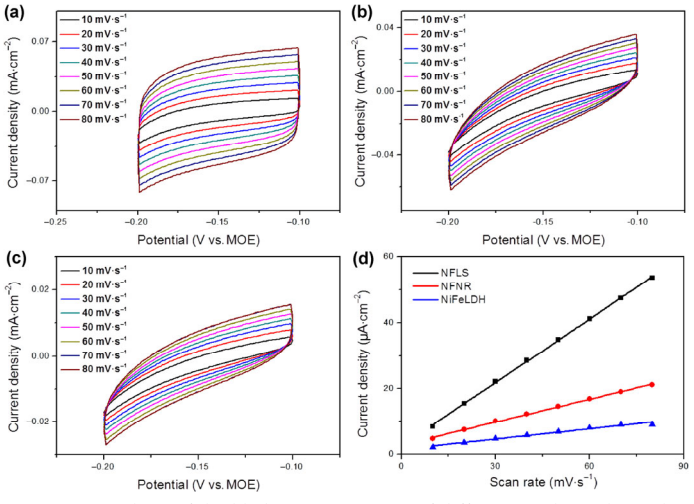

Figure 5 Analysis of double layer capacitance of different working electrodes. CV curves of (a) NFLS, (b) NFNR and (c) NiFeLDH bulk with different scanning rates in 1 M KOH electrolyte around open-circuit. (d) Linear regression of scan rate against current density. The slope of regression curves stands for the double layer capacitance density.

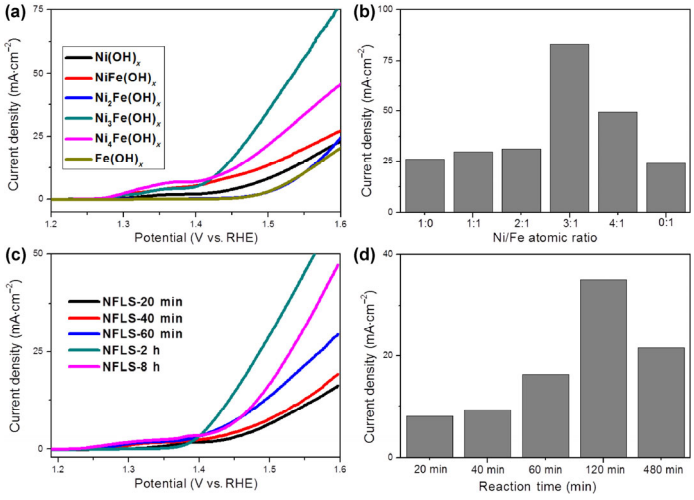

Figure 6 Controlled experiment of different catalyst preparatory condition on OER overpotential. (a) LSV curves toward OER in the present of NFLS with different ratio of Ni and Fe, together with $Ni(OH)_2$ and $Fe(OH)_3$ as controling group. (b) Current densities of different ratio of Ni and Fe at an overpotential of 400 mV. (c) LSV curves toward OER in the present of NFLS with different hydrothermal reaction time. (d) Current densities of different reaction time at an overpotential of 300 mV.

Acknowledgements

This work was supported by the National Natural Science Foundation of China (Nos. 21431003 and 21521091) and the National Key Technology R&D Program of China (No. 2016YFA0202801).

Electronic Supplementary Material: Supplementary material (experimental details and additional SEM, TEM images) is available in the online version of this article at https://doi.org/10.1007/s12274-019-2284-0.

References

[1] Yang, Y.; Yang, Y.; Chen, S. M.; Lu, Q. C.; Song, L.; Wei, Y.; Wang, X. Atomic-level molybdenum oxide nanorings with full-spectrum absorption and photoresponsive properties. *Nat. Commun.* **2017**, *8*, 1559.

[2] Hu, S.; Wang, X. Ultrathin nanostructures: Smaller size with new phenomena. *Chem. Soc. Rev.* **2013**, *42*, 5577–5594.

[3] Gu, C. D.; Ge, X.; Wang, X. L.; Tu, J. P. Cation-anion double hydrolysis derived layered single metal hydroxide superstructures for boosted supercapacitive energy storage. *J. Mater. Chem. A* **2015**, *3*, 14228–14238.

[4] Wang, Q.; O'Hare, D. Recent advances in the synthesis and application of layered double hydroxide (LDH) nanosheets. *Chem. Rev.* **2012**, *112*, 4124–4155.

[5] Song, F.; Hu, X. L. Exfoliation of layered double hydroxides for enhanced oxygen evolution catalysis. *Nat. Commun.* **2014**, *5*, 4477.

[6] Ma, W.; Ma, R. Z.; Wang, C. X.; Liang, J. B.; Liu, X. H.; Zhou, K. C.; Sasaki, T. A superlattice of alternately stacked Ni-Fe hydroxide nanosheets and graphene for efficient splitting of water. *ACS Nano* **2015**, *9*, 1977–1984.

[7] Andronescu, C.; Barwe, S.; Ventosa, E.; Masa, J.; Vasile, E.; Konkena, B.; Möller, S.; Schuhmann, W. Powder catalyst fixation for post-electrolysis structural characterization of NiFe layered double hydroxide based oxygen evolution reaction electrocatalysts. *Angew. Chem., Int. Ed.* **2017**, *56*, 11258–11262.

[8] Wang, Y. Y.; Zhang, Y. Q.; Liu, Z. J.; Xie, C.; Feng, S.; Liu, D. D.; Shao, M. F.; Wang, S. Y. Layered double hydroxide nanosheets with multiple vacancies obtained by dry exfoliation as highly efficient oxygen evolution electrocatalysts. *Angew. Chem., Int. Ed.* **2017**, *56*, 5867–5871.

[9] Song, F.; Hu, X. L. Ultrathin cobalt-manganese layered double hydroxide is an efficient oxygen evolution catalyst. *J. Am. Chem. Soc.* **2014**, *136*, 16481–16484.

[10] Han, N.; Zhao, F. P.; Li, Y. G. Ultrathin nickel-iron layered double hydroxide nanosheets intercalated with molybdate anions for electrocatalytic water oxidation. *J. Mater. Chem. A* **2015**, *3*, 16348–16353.
[11] Zou, X. X.; Zhang, Y. Noble metal-free hydrogen evolution catalysts for water splitting. *Chem. Soc. Rev.* **2015**, *44*, 5148–5180.
[12] Shi, Y. M.; Zhang, B. Recent advances in transition metal phosphide nanomaterials: Synthesis and applications in hydrogen evolution reaction. *Chem. Soc. Rev.* **2016**, *45*, 1781–1781.
[13] Yang, J. H.; Cooper, J. K.; Toma, F. M.; Walczak, K. A.; Favaro, M.; Beeman, J. W.; Hess, L. H.; Wang, C.; Zhu, C. H.; Gul, S. et al. A multifunctional biphasic water splitting catalyst tailored for integration with high-performance semiconductor photoanodes. *Nat. Mater.* **2017**, *16*, 335–341.
[14] Long, X.; Li, J. K.; Xiao, S.; Yan, K. Y.; Wang, Z. L.; Chen, H. N.; Yang, S. H. A strongly coupled graphene and feni double hydroxide hybrid as an excellent electrocatalyst for the oxygen evolution reaction. *Angew. Chem., Int. Ed.* **2014**, *53*, 7584–7588.
[15] Ma, T. Y.; Dai, S.; Jaroniec, M.; Qiao, S. Z. Metal-organic framework derived hybrid Co_3O_4-carbon porous nanowire arrays as reversible oxygen evolution electrodes. *J. Am. Chem. Soc.* **2014**, *136*, 13925–13931.
[16] Zhang, B.; Zheng, X. L.; Voznyy, O.; Comin, R.; Bajdich, M.; García-Melchor, M.; Han, L. L.; Xu, J. X.; Liu, M.; Zheng, L. R. et al. Homogeneously dispersed multimetal oxygen-evolving catalysts. *Science* **2016**, *352*, 333–337.
[17] Ge, X. M.; Liu, Y. Y.; Goh, F. W. T.; Hor, T. S. A.; Zong, Y.; Xiao, P.; Zhang, Z.; Lim, S. H.; Li, B.; Wang, X. et al. Dual-phase spinel $MnCo_2O_4$ and spinel $MnCo_2O_4$/nanocarbon hybrids for electrocatalytic oxygen reduction and evolution. *ACS Appl. Mater. Interfaces* **2014**, *6*, 12684–12691.
[18] Li, Y. Y.; Liu, B.; Wang, H.; Su, X. S.; Gao, L.; Zhou, F.; Duan, G. T. Co_3O_4 nanosheet-built hollow dodecahedrons via a two-step self-templated method and their multifunctional applications. *Sci. China Mater.* **2018**, *61*, 1575–1586.
[19] Guo, Y.; Yao, Y.; Li, H.; He, L. L.; Zhu, Z. W.; Yang, Z. Z.; Gong, L. D.; Liu, C.; Zhao, D. X. Theoretical study on the mechanism of photosynthetic oxygen evolution by ABEEM/MM/MD and BS-DFT. *Acta Chim. Sin.* **2017**, *75*, 903–913.
[20] Gao, M. R.; Sheng, W. C.; Zhuang, Z. B.; Fang, Q. R.; Gu, S.; Jiang, J.; Yan, Y. S. Efficient water oxidation using nanostructured α-nickel-hydroxide as an electrocatalyst. *J. Am. Chem. Soc.* **2014**, *136*, 7077–7084.
[21] Tang, C.; Wang, H. S.; Wang, H. F.; Zhang, Q.; Tian, G. L.; Nie, J. Q.; Wei, F. Spatially confined hybridization of nanometer-sized NiFe hydroxides into nitrogen-doped graphene frameworks leading to superior oxygen evolution reactivity. *Adv. Mater.* **2015**, *27*, 4516–4522.
[22] Zhang, Y. Q.; Ouyang, B.; Xu, J.; Jia, G. C.; Chen, S.; Rawat, R. S.; Fan, H. J. Rapid synthesis of cobalt nitride nanowires: Highly efficient and low-cost catalysts for oxygen evolution. *Angew. Chem., Int. Ed.* **2016**, *55*, 8670–8674.
[23] Wang, Y. Y.; Xie, C.; Liu, D. D.; Huang, X. B.; Huo, J.; Wang, S. Y. Nanoparticle-stacked porous nickel-iron nitride nanosheet: A highly efficient bifunctional electrocatalyst for overall water splitting. *ACS Appl. Mater. Interfaces* **2016**, *8*, 18652–18657.
[24] Jia, X. D.; Zhao, Y. F.; Chen, G. B.; Shang, L.; Shi, R.; Kang, X. F.; Waterhouse, G. I. N.; Wu, L. Z.; Tung, C. H.; Zhang, T. R. Ni_3FeN nanoparticles derived from ultrathin NiFe-layered double hydroxide nanosheets: An efficient overall water splitting electrocatalyst. *Adv. Energy Mater.* **2016**, *6*, 1502585.
[25] Swesi, A. T.; Masud, J.; Nath, M. Nickel selenide as a high-efficiency catalyst for oxygen evolution reaction. *Energy Environ. Sci.* **2016**, *9*, 1771–1782.
[26] Xu, X.; Song, F.; Hu, X. L. A nickel iron diselenide-derived efficient oxygen-evolution catalyst. *Nat. Commun.* **2016**, *7*, 12324.
[27] Wang, C. D.; Jiang, J.; Ding, T.; Chen, G. H.; Xu, W. J.; Yang, Q. Monodisperse ternary NiCoP nanostructures as a bifunctional electrocatalyst for both hydrogen and oxygen evolution reactions with excellent performance. *Adv. Mater. Interfaces* **2016**, *3*, 1500454.
[28] Pramanik, M.; Li, C. L.; Imura, M.; Malgras, V.; Kang, Y. M.; Yamauchi, Y. Ordered mesoporous cobalt phosphate with crystallized walls toward highly active water oxidation electrocatalysts. *Small* **2016**, *12*, 1709–1715.
[29] Liu, M. J.; Li, J. H. Cobalt phosphide hollow polyhedron as efficient bifunctional electrocatalysts for the evolution reaction of hydrogen and oxygen. *ACS Appl. Mater. Interfaces* **2016**, *8*, 2158–2165.
[30] He, P. L.; Yu, X. Y.; Lou, X. W. Carbon-incorporated nickel-cobalt mixed metal phosphide nanoboxes with enhanced electrocatalytic activity for oxygen evolution. *Angew. Chem., Int. Ed.* **2017**, *56*, 3897–3900.
[31] Chi, J.; Yu, H. M.; Qin, B. W.; Fu, L.; Jia, J.; Yi, B. L.; Shao, Z. G. Vertically aligned FeOOH/NiFe layered double hydroxides electrode for highly efficient oxygen evolution reaction. *ACS Appl. Mater. Interfaces* **2017**, *9*, 464–471.
[32] Zhang, C.; Shao, M. F.; Zhou, L.; Li, Z. H.; Xiao, K. M.; Wei, M. Hierarchical NiFe layered double hydroxide hollow microspheres with highly-efficient behavior toward oxygen evolution reaction. *ACS Appl. Mater. Interfaces* **2016**, *8*, 33697–33703.
[33] Zhou, D. J.; Cai, Z.; Bi, Y. M.; Tian, W. L.; Luo, M.; Zhang, Q.; Zhang, Q.; Xie, Q. X.; Wang, J. D.; Li, Y. P. et al. Effects of redox-active interlayer anions on the oxygen evolution reactivity of NiFe-layered double hydroxide nanosheets. *Nano Res.* **2018**, *11*, 1358–1368.
[34] Tang, D.; Liu, J.; Wu, X. Y.; Liu, R. H.; Han, X.; Han, Y. Z.; Huang, H.; Liu, Y.; Kang, Z. H. Carbon quantum Dot/NiFe layered double-hydroxide composite as a highly efficient electrocatalyst for water oxidation. *ACS Appl. Mater. Interfaces* **2014**, *6*, 7918–7925.
[35] Xiong, X. Y.; Cai, Z.; Zhou, D. J.; Zhang, G. X.; Zhang, Q.; Jia, Y.; Duan, X. X.; Xie, Q. X.; Lai, S. B.; Xie, T. H. et al. A highly-efficient oxygen evolution electrode based on defective nickel-iron layered double hydroxide. *Sci. China Mater.* **2018**, *61*, 939–947.
[36] Ma, J. Z.; Xiang, Z. H.; Zhang, J. T. Three-dimensional nitrogen and phosphorous Co-doped graphene aerogel electrocatalysts for efficient oxygen reduction reaction. *Sci. China Chem.* **2018**, *61*, 592–597.
[37] Gong, M.; Li, Y. G.; Wang, H. L.; Liang, Y. Y.; Wu, J. Z.; Zhou, J. G.; Wang, J.; Regier, T.; Wei, F.; Dai, H. J. An advanced Ni-Fe layered double hydroxide electrocatalyst for water oxidation. *J. Am. Chem. Soc.* **2013**, *135*, 8452–8455.
[38] Friebel, D.; Louie, M. W.; Bajdich, M.; Sanwald, K. E.; Cai, Y.; Wise, A. M.; Cheng, M. J.; Sokaras, D.; Weng, T. C.; Alonso-Mori, R. et al. Identification of highly active Fe sites in (Ni,Fe)OOH for electrocatalytic water splitting. *J. Am. Chem. Soc.* **2015**, *137*, 1305–1313.
[39] Trotochaud, L.; Young, S. L.; Ranney, J. K.; Boettcher, S. W. Nickel-iron oxyhydroxide oxygen-evolution electrocatalysts: The role of intentional and incidental iron incorporation. *J. Am. Chem. Soc.* **2014**, *136*, 6744–6753.
[40] Yeo, B. S.; Bell, A. T. Enhanced activity of gold-supported cobalt oxide for the electrochemical evolution of oxygen. *J. Am. Chem. Soc.* **2011**, *133*, 5587–5593.
[41] Parvulescu, A. N.; Hausoul, P. J. C.; Bruijnincx, P. C. A.; Korhonen, S. T.; Teodorescu, C.; Gebbink, R. J. M. K.; Weckhuysen, B. M. Telomerization of 1,3-butadiene with biomass-derived alcohols over a heterogeneous Pd/TPPTS catalyst based on layered double hydroxides. *ACS Catal.* **2011**, *1*, 526–536.
[42] Liu, Z. P.; Ma, R. Z.; Osada, M.; Iyi, N.; Ebina, Y.; Takada, K.; Sasaki, T. Synthesis, anion exchange, and delamination of Co-Al layered double hydroxide: Assembly of the exfoliated nanosheet/polyanion composite films and magneto-optical studies. *J. Am. Chem. Soc.* **2006**, *128*, 4872–4880.
[43] Yu, L.; Zhou, H. Q.; Sun, J. Y.; Qin, F.; Yu, F.; Bao, J. M.; Yu, Y.; Chen, S.; Ren, Z. F. Cu nanowires shelled with NiFe layered double hydroxide nanosheets as bifunctional electrocatalysts for overall water splitting. *Energy Environ. Sci.* **2017**, *10*, 1820–1827.
[44] Ni, B.; He, T.; Wang, J. O.; Zhang, S. M.; Ouyang, C.; Long, Y.; Zhuang, J.; Wang, X. The formation of $(NiFe)S_2$ pyrite mesocrystals as efficient pre-catalysts for water oxidation. *Chem. Sci.* **2018**, *9*, 2762–2767.
[45] Smith, R. D. L.; Prévot, M. S.; Fagan, R. D.; Trudel, S.; Berlinguette, C. P. Water oxidation catalysis: Electrocatalytic response to metal stoichiometry in amorphous metal oxide films containing iron, cobalt, and nickel. *J. Am. Chem. Soc.* **2013**, *135*, 11580–11586.
[46] Xu, K.; Chen, P. Z.; Li, X. L.; Tong, Y.; Ding, H.; Wu, X. J.; Chu, W. S.; Peng, Z. M.; Wu, C. Z.; Xie, Y. Metallic nickel nitride nanosheets realizing enhanced electrochemical water oxidation. *J. Am. Chem. Soc.* **2015**, *137*, 4119–4125.
[47] Cheng, Y.; Dou, S.; Saunders, M.; Zhang, J.; Pan, J.; Wang, S. Y.; Jiang, S. P. A class of transition metal-oxide@MnO_x core-shell structured oxygen electrocatalysts for reversible O_2 reduction and evolution reactions. *J. Mater. Chem. A* **2016**, *4*, 13881–13889.
[48] Hou, J. G.; Sun, Y. Q.; Cao, S. Y.; Wu, Y. Z.; Chen, H.; Sun, L. C. Graphene dots embedded phosphide nanosheet-assembled tubular arrays for efficient and stable overall water splitting. *ACS Appl. Mater. Interfaces* **2017**, *9*, 24600–24607.
[49] Kibsgaard, J.; Jaramillo, T. F. Molybdenum phosphosulfide: An active, acid-stable, earth-abundant catalyst for the hydrogen evolution reaction. *Angew. Chem., Int. Ed.* **2014**, *53*, 14433–14437.